Seismicity near the slip maximum of the 1960 Mw 9.5 Valdivia earthquake (Chile): Plate interface lock and reactivation of the subducted Valdivia Fracture Zone

Yvonne Dzierma,[1] Martin Thorwart,[1] Wolfgang Rabbel,[1] Claudia Siegmund,[1] Diana Comte,[2] Klaus Bataille,[3] Paula Iglesia,[4] and Claudia Prezzi[4]

Received 10 October 2011; revised 5 April 2012; accepted 26 April 2012; published 23 June 2012.

[1] Understanding the processes behind subduction-related hazards is an important responsibility and major challenge for the Earth sciences. Few areas demonstrate this as clearly as south-central Chile, where some of the largest earthquakes in human history have occurred. We present the first observation of local seismicity in the Villarrica region (39°–40°S), based on a temporary local network of 55 stations installed from the Chilean coast into the Argentinian back-arc for one year. While consistent with the Chilean national catalog (SSN), our results allow us to observe smaller magnitudes with a completeness of about 2.0 and image the geometry of the Wadati-Benioff Zone from the Chile Trench down to 200 km. Offshore, a gap in interplate seismicity is observed in the region of the 1960 Valdivia earthquake slip. Above the interface, two offshore seismicity clusters possibly indicate ongoing stress relaxation. In the subducting Nazca Plate, we find a prominent seismicity cluster along the extrapolated trace of the oceanic Valdivia Fracture Zone (VFZ). The seismicity cluster is observed between 70 and 130 km depth and comprises mainly strike-slip events. It indicates weakening and reactivation of the major VFZ by dehydration of oceanic crust and mantle. Interpreting the subducted VFZ section as a localized reservoir of potential fluid release offers an explanation for the Villarrica volcanic complex that is located above the reactivated VFZ and shows the highest volcanic activity in South America. Crustal seismicity is observed near Puyehue volcano, which recently started to erupt (June 2011).

Citation: Dzierma, Y., M. Thorwart, W. Rabbel, C. Siegmund, D. Comte, K. Bataille, P. Iglesia, and C. Prezzi (2012), Seismicity near the slip maximum of the 1960 Mw 9.5 Valdivia earthquake (Chile): Plate interface lock and reactivation of the subducted Valdivia Fracture Zone, *J. Geophys. Res.*, *117*, B06312, doi:10.1029/2011JB008914.

1. Introduction

[2] Strong tsunami generating earthquakes belong to the most hazardous geodynamic processes occurring along the world's plate margins. The South-Central Chilean subduction zone is known for having produced some of the largest observed earthquakes - among them, the greatest instrumentally recorded earthquake, the 1960 Mw 9.5 Valdivia event [*Barrientos and Ward*, 1990; *Cifuentes*, 1989] - and has recently ruptured again during the 2010 Mv 8.8 Maule earthquake and aftershock sequence [*Delouis et al.*, 2010]. In addition to a particularly high potential for large interseismic strain accumulation, this region is home to some of South America's most active volcanoes, Llaima and Villarrica [*Stern*, 2004].

[3] The geometry and geophysical properties of this subduction system are well constrained north of 39°S and south of 41°S, but not in between, where the 1960 coseismic slip was greatest (between 39°S and 40°S). Although broad similarities with the north and south adjacent regions are observed, the region between 39°S and 40°S (but not between 40°S and 41°S) is found to be very different in geomorphology and gravity [*Hackney et al.*, 2006; *Rehak et al.*, 2008; *Alasonati Tasarova*, 2007], and has been speculated to present a different stress regime. On the basis of the gravity measurements, it was hypothesized that plate coupling in this segment of the subduction zone is stronger than in the adjacent regions [*Hackney et al.*, 2006]. Conversely, GPS measurements suggest that plate locking is reduced between the incoming Valdivia and Mocha fracture zones [*Moreno et al.*, 2011]. This apparent controversy may actually be due to the different time scales considered: the gravity signature will be stable over geological times,

[1]SFB 574, Institute of Geosciences, Department of Geophysics, Christian-Albrechts University Kiel, Kiel, Germany.
[2]Departamento de Geofísica, Universidad de Chile, Santiago, Chile.
[3]Departamento de Ciencias de la Tierra, Universidad de Concepción, Concepción, Chile.
[4]CONICET, Departamento de Ciencias Geológicas, Facultad de Ciencias Exactas y Naturales, Universidad de Buenos Aires, Buenos Aires, Argentina.

Corresponding author: M. Thorwart, SFB 574, Institute of Geosciences, Department of Geophysics, Christian-Albrechts University Kiel, Otto-Hahn-Platz 1, D-24118 Kiel, Germany. (thorwart@geophysik.uni-kiel.de)

0148-0227/12/2011JB008914

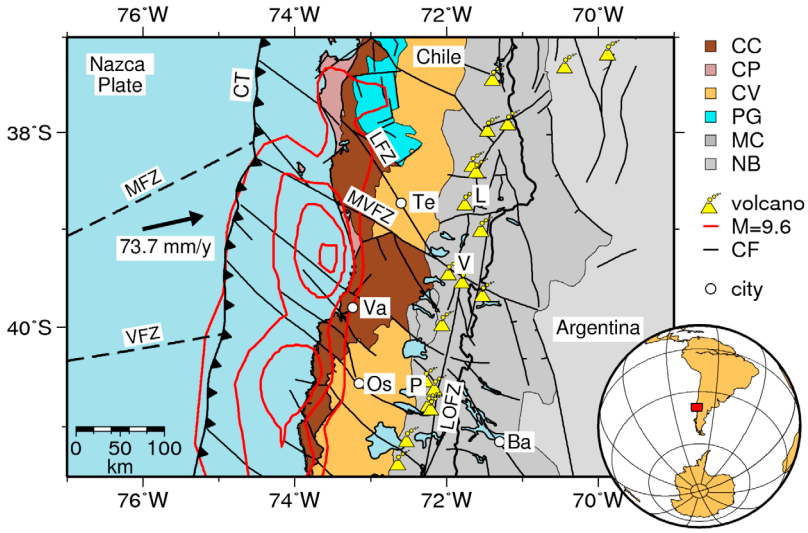

Figure 1. Tectonic overview of the investigation area. Geologic units: CC - Coastal Cordillera, CP - Coastal Platform, CV - Central Valley, PG - Paleozoic Granites, MC - Main Cordillera and NB - Neuquén Basin. Red contour lines indicate the slip distribution of the 1960 M = 9.6 earthquake for 5 m, 15 m, 25 m and 35 m [*Barrientos and Ward*, 1990]. Black lines show crustal faults (CF) [*Melnick and Echtler*, 2006]. Major faults: LOFZ - Liquiñe-Ofqui-fault zone, MVFZ - Mocha-Villarrica-fault zone, LFZ - Lanalhue fault zone, MFZ - Mocha fracture zone and VFZ - Valdivia fracture zone. Main volcanoes: V - Villarrica, L - Llaima, P - Puyehue-Cordón Caulle. Major cities shown: Te - Temuco, Va - Valdivia, Os - Osorno and Ba - Bariloche. The black arrow indicates the convergence rate of 73.7 mm/y and direction of the Nazca Plate relative to the South American Plate.

whereas the GPS measurements look at the instantaneous locking. In any case, the marked contrast between this segment and the surrounding regions make it a key region for understanding subduction-related processes along this plate margin.

[4] This region has not been subject to regional seismological studies because it was believed to exhibit no significant seismic activity, due to the scarcity of local earthquakes registered in this region both by international networks (IRIS-NEIC, http://earthquake.usgs.gov/earthquakes/) and the Chilean National Seismological Service (SSN, http://ssn.dgf.uchile.cl/). However, while this region may actually be seismically quiet due to plate-locking at the interface following the last great earthquake [*Hu et al.*, 2004; *Khazaradze et al.*, 2002], the observed lack of seismicity may also be artificially induced by station coverage. We here present results from a temporal local network of 55 stations installed between 39°S and 40°S, covering the area from the Chilean coast to the back-arc in Argentina.

[5] The main aims of the study are: first, to verify if the local and regional seismicity in this region is really subdued, which has important implications for seismic locking and strain buildup along the plate interface. Recently, *Moreno et al.* [2011] have suggested that the 1960 slip interface is locked and building up stress for the next large earthquake and also suggested that locking is only partial along the trace of the subducting Valdivia Fracture Zone. We test this hypothesis by investigating the local seismicity distribution along the 1960 slip interface. Second, we aim to resolve the deep structure of the Wadati-Benioff-Zone, which is unconstrained in this region because the international catalog data does not delineate a dipping slab even when considered over several decades. The intermediate depth seismicity along the Wadati-Benioff Zone is an important indicator for dehydration reactions of the subducting plate crust and mantle, which in turn feed the volcanic arc. Since the study region is home to one of the most active volcanoes of the Chilean Southern Volcanic Zone, a primary goal of our work is to investigate the dehydration of the downgoing slab and possible influences of the subducting fracture zones on fluid release and pathways. Third, the regional character of this study will allow us to determine the relevance of active fault zones geologically observed in the overriding plate and the activity of the volcanic centers.

2. Tectonic Framework and Previous Studies

[6] In the study region (Figure 1), the Nazca Plate subducts obliquely (77.5°) beneath the South American Plate with a convergence velocity of 73.7 mm/yr [*DeMets et al.*, 2010]. The downgoing slab is cut by several transform faults, the most prominent of which is the Valdivia Fracture Zone (VFZ) impinging on the trench at 40°S. The VFZ constitutes the boundary between ~26 Ma oceanic crust produced at the East Pacific Rise and younger (18–20 Ma) crust produced at the Chile Rise in the south [*Tebbens et al.*, 1997].

[7] As a result of oblique subduction, a large crustal forearc sliver has formed, bounded to the east by the Liquiñe-Ofqui Fault Zone (LOFZ), a 1100 km long trench-parallel slip system [*Cembrano et al.*, 2000; *Rosenau et al.*, 2006]. Together with a number of WNW-trending fault zones in the overriding plate (most prominently in this area, the Mocha-Villarrica Fault Zone, MVFZ [*Melnick and Echtler*, 2006]), this system of active faults is a major determinant for the position of the active volcanic centers [*Cembrano and Lara*, 2009].

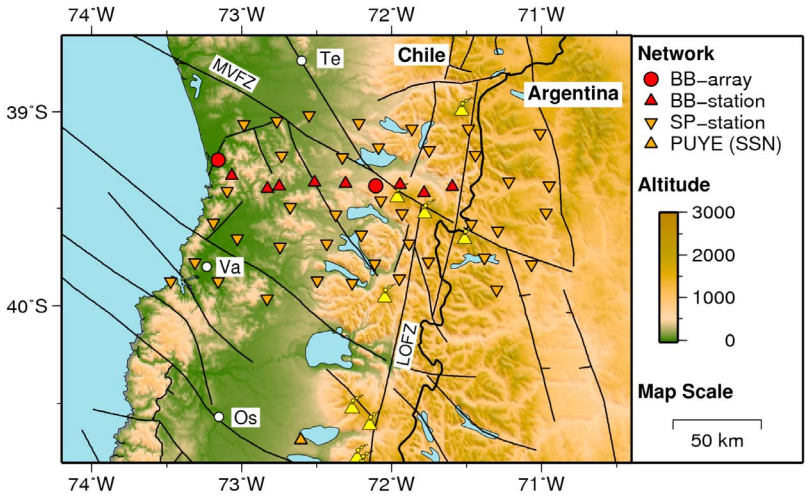

Figure 2. Location map of the seismic network. Seismic installations: BB-Ar - Array of broadband stations, BB-St - single broadband stations and SP-St - single short period stations. Faults, volcanoes and cities are the same as in Figure 1.

[8] From a morphotectonic point of view, the overriding plate is segmented into three main units (from west to east): the Coastal Cordillera, Central Valley, and Main Cordillera, where the active volcanic arc is located [see, e.g., *Charrier et al.*, 2007]. From surface geology observations, the Central Valley seems to be absent in the Villarrica region between 39 and 40°S. In addition to the atypical surface geology, this region is found to exhibit an unusual negative Bouguer gravity anomaly of 0 to −50 mGal, which contrasts with the positive anomalies found to either side of this region and along the rest of the margin [*Hackney et al.*, 2006]. The boundaries of the anomalous Villarrica segment defined by *Hackney et al.* [2006] coincide to the north with the MVFZ, while to the south they occur along a parallel-trending line through the Puyehue-Cordón Caulle volcano group.

[9] Studies of the seismicity to the north (36°–39°S [*Bohm et al.*, 2002; *Haberland et al.*, 2006]) of the study region identified the Wadati-Benioff Zone down to 120 km depth with a dip of 30°E. While observing some crustal seismicity in the northern part of their study area, they found almost no crustal seismicity in the southern sector. In the Chiloé region (41.5°–43.5°S), *Lange et al.* [2007] observed a 30° dipping Wadati-Benioff zone down to a depth of 70 km and crustal seismicity in several clusters associated with the volcanic arc.

3. Data Basis and Determination of Hypocenters

3.1. Field Data and Travel Times

[10] A network consisting of 15 broadband stations (Güralp 3ESP-60s) and 40 short-period stations (Mark L-4C-3D) was operated for one year from December 2008 to November 2009 in the area between 39°S and 40°S in north-south direction, and from the Pacific coast to 71°W in east-west direction (Figure 2 and Table S1).[1] In addition, the Chilean National Seismological Service (SSN) provided continuous seismic recordings of station PUYE located 80 km south of our network and west of the volcanic complex of Puyehue-Cordón Caulle.

[11] In order to identify seismic events we applied an STA/LTA trigger algorithm, followed by a network trigger, to the continuous field records resulting in 2350 possible events (Table 1). Based on this information, P- and S-wave onset times and amplitudes were then picked interactively using the SEISAN software package [*Havskov and Ottemöller*, 1999]. For 11 events between 38.5°S and 41.0°S travel time picks of SSN stations were available and added to the data basis as additional constraints for the determination of hypocenters. Most of these SSN stations are located north and at greater distances. The determination of hypocenters was performed in a two-step procedure of single event and double difference location.

3.2. Single Event Locations and Magnitude Completeness

[12] In the first step the events were located by applying a single event approach (computer program HYPOCENTER by *Lienert et al.* [1986,1991,1995]) based on the optimum 1D velocity model of *Haberland et al.* [2006] (Table 2). This model was originally determined for the region north of our investigation area (37°S to 39°S). However, test computations of a joint hypocenter-velocity inversion (computer program VELEST by *Kissling et al.* [1994] ftp://ftp.ingv.it/pub/mario.anselmi/velest.pdf) showed that it applies well to our field site, too. Indeed, optimum 1D velocity models

Table 1. Parameters for Single-Station Triggering and Net-Triggering

Parameter	Value
Single-Station Triggering	
STA – length	0.5 s
LTA – length	8.0 s
Trigger – threshold	5
Lower frequency	1.5 Hz
Upper frequency	10. Hz
Net-Triggering	
Window – length	15. s
Min. Number of stations	6

[1]Auxiliary materials are available in the HTML. doi:10.1029/2011JB008914.

Table 2. One Dimensional Velocity-Depth Model Used for Hypocenter Location From *Haberland et al.* [2006]

Depth to Bottom of Layer (km)	P Wave Velocity (km/s)	S Wave Velocity (km/s)
0.0	4.900	2.750
1.0	6.100	3.420
5.0	6.300	3.540
9.0	6.500	3.650
10.0	6.600	3.700
16.0	6.700	3.760
30.0 (Moho)	7.300	4.100
50.0	7.900	4.440
400.0	8.100	4.550

computed for the new data did not show any improvement compared to the 1D-model of *Haberland et al.* [2006] which was, therefore, selected in order to remain regionally compatible. Station corrections were calculated from the altitude and the velocity of the uppermost layer.

[13] Based on single event locations we identified a total of 867 local and regional events of local magnitudes up to 4.4 at epicentral distances less than 500 km. 630 hypocenter locations of these were classified as "reliable" based on the criterion that they showed rms-residuals of less than 1 s. These events have a median rms-residual of 0.3 s (Figure 3). Figure 4 shows the spatial distribution of location errors corresponding to the rms-residuals. It shows both horizontal and vertical location errors based on single event locations computed with the program HYPOCENTER by *Lienert et al.* [1986, 1991, 1995]). The maps were smoothed by computing and plotting medians in a moving window. Location errors of individual events can be identified by the color of the dots. The location errors are smaller than 5 km beneath the network and adjacent areas 50 km to the north and south (that is from 38.5°S to 40.5°S), and generally smaller than 10 km (with only few exceptions) between 38°S and 41°S.

[14] The magnitude-frequency relation of the events with reliable hypocenters in the area between 39°S and 40°S and between 74°W and 71°W is shown in Figure 5. Local magnitudes ML were determined with the respective SEISAN module [*Havskov and Ottemöller*, 1999]. The Chilean seismic agency SSN reports local magnitudes to the International Seismological Center (ISC) since November 2001. The diagram (Figure 5) shows that the statistics of the events recorded by our network agrees basically with the 8 years spanning catalog of SSN data. We find a small deviation in the a-value because no events of ML $\geq$ 4.5 occurred during the deployment time of our network. Figure 5 shows that our recordings are complete to a minimum magnitude of ca. 2. Single event locations are shown in Figure 6.

3.3. Double Difference Location and Determination of Seismicity Clusters

[15] In a second step we applied the double difference location of *Waldhauser and Ellsworth* [2000] (computer program hypoDD by *Waldhauser* [2001]) in order to improve the relative locations of the hypocenters and to identify spatial seismicity clusters. Only the catalog data (picked onset-times and coordinates, no waveforms) of the 630 reliable events were used for input. The hypoDD algorithm allows to search for clustering within the input data. The clustering analysis is sensitive to the maximum separation between neighboring events. We limited the maximum separation of the hypocenters of event pairs to 15 km but applied no restriction to the allowed hypocenter-station distances. Using the least square (LSQR) solver option of hypoDD to identify spatial seismicity clusters, we found 16 major clusters which are stable for maximum separation parameters from ~5 to ~15 km. For a maximum separation parameter larger than 20 km the complete Wadati-Benioff-zone would be seen as one large cluster. For a maximum separation smaller ~5 km the major clusters would be divided into several subclusters. Since the LSQR solver underestimates the location errors [*Waldhauser*, 2001] clusters of special interest were relocated separately using the singular value decomposition (SVD) solver of hypoDD.

[16] The double difference algorithm assigned ~60% (358/630) of the input events to spatial clusters. About 2/3 of these clustered events (224/358) fall into the 16 biggest clusters that comprise a minimum of 6 events each. Nine of these bigger clusters (Figure 7) can be recognized directly in the hypocenter diagram based on the first single event locations (Figure 6).

4. Results

4.1. Overall Seismicity

[17] Most of the earthquakes were observed between 38°S and 41°S (single event location Figure 6); outside this region the observations decrease rapidly. About 50% (302) of the events were located in the presumed seismically quiet zone between 39°S and 40°S where the seismic network had been deployed. About 2/3 of the remaining 50% of events were observed north of the network between 38 and 39°S indicating a decrease of seismic activity from North to South.

[18] During the same time period the USGS NEIC global catalog lists only 3 events. This is mainly due to the comparatively small magnitude of the events (<3.5 inside the

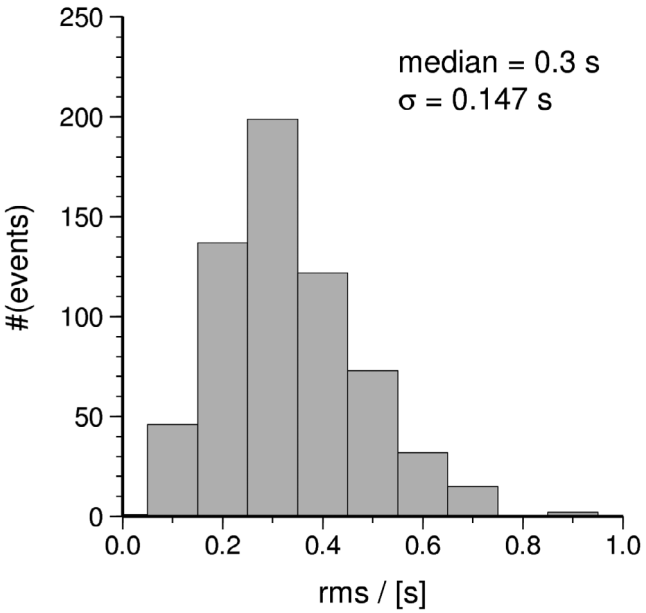

Figure 3. RMS travel time residuals after relocation for the 630 microseismic events used in this study. The median value is 0.3 s, the standard deviation is 0.147 s.

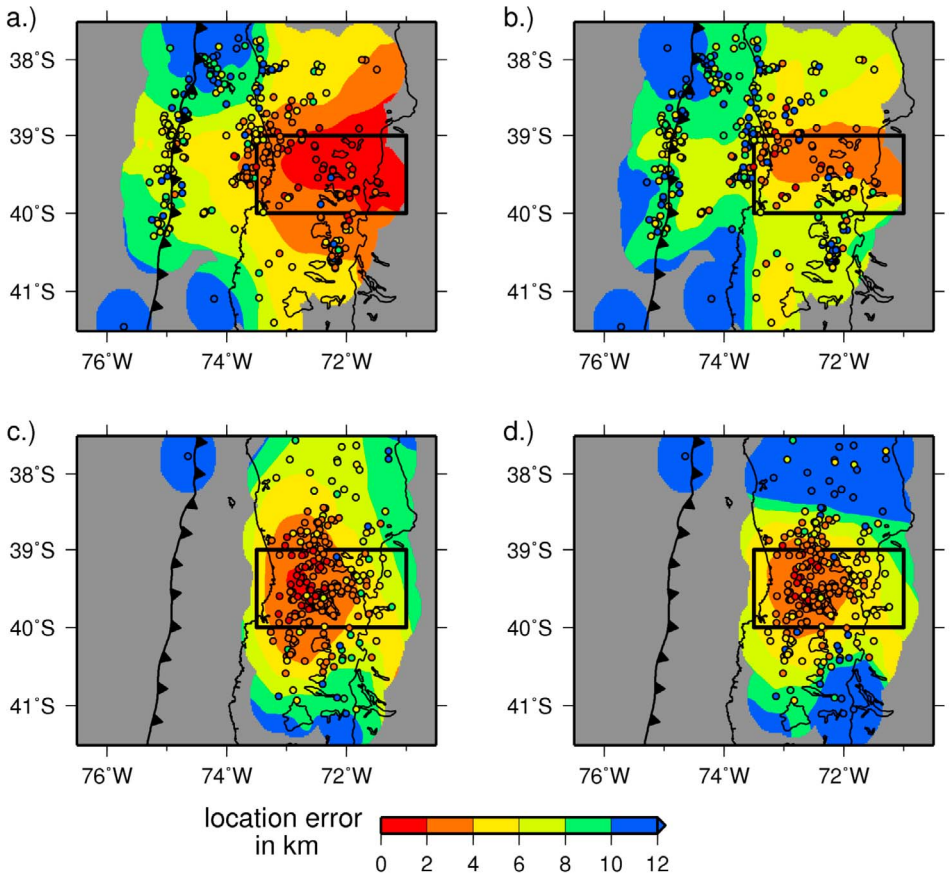

Figure 4. Location errors of the 630 events used in this study. The errors correspond to the rms-traveltime residuals of single event locations: (a) horizontal location error and (b) depth error for shallow events (depth < 50 km); (c) horizontal location error and (d) depth error for deep events (depth > 50 km). The color of the dots shows the location errors of single events, the background color is a smoothed interpolation. The black box indicates the network area.

network), which is below detection limit of the global networks. The magnitude of completeness for our temporal network is ~2.0, compared with about 4.0 of the SSN catalog (Figure 5). Despite the very different magnitude of observed events, the Gutenberg-Richter statistics of events from our network agrees well with the SSN observations (Figure 5). The smaller magnitude of completeness allows us to present the first image of the Wadati-Benioff Zone seismicity and local seismic activity in the Villarrica region.

[19] The Wadati-Benioff zone is well delineated by the deeper seismicity down to a depth of almost 200 km (Figure 6, profiles P1–P3). The dip angle of the intermediate-depth events defining the Wadati-Benioff zone is approximately 15° down to 60 km depth and increases gradually to 45° at maximum depth. The plate interface is nearly void of events between ~10 and 30 km depth where the maximum slip of the 1990 Mw9.5 Valdivia earthquake occurred. Seismicity is observed again at the shallow part of the plate interface near the trench where it is probably caused by bending-related faulting. The seismicity of the overriding continent (red dots east of the coastline, Figure 6) concentrates mainly along the volcanic arc and the coinciding Liquiñe-Ofqui Fault Zone and appears rather diffuse elsewhere.

[20] The cluster analysis inherent in the double difference location method revealed that about 60% of the observed events form groups with a hypocenter spacing of ~15 km. Actually, 40% of all events are grouped in only a small number of major clusters. Therefore, we regard earthquake clustering as a characteristic of the Villarrica section of the subduction zone. The most evident major clusters are labeled A to H in Figures 6 and 7 and are described in the following.

4.2. Spatial Seismicity Clusters

[21] In the map and the vertical sections parallel and perpendicular to the trench (Figure 6) we observe major seismicity clusters in the deeper slab (A), near the trench (C, D), near the maximum slip of the 1960 earthquake (E, F) and in the overriding plate (G, H). These clusters, shown isolated from the background seismicity in Figure 7, were selected for a separate more precise relative location with the double difference method and their differences to the single event location which are generally small. (Figures 8 and 9).

4.2.1. Valdivia Fault Zone Cluster (Clusters A and B)

[22] The earthquakes of clusters A and its subcluster B form a streak in the downgoing slab at a depth between 80 and 110 km (Figure 8). This streak extends within a 30 km wide band along the downdip extrapolation of the Valdivia

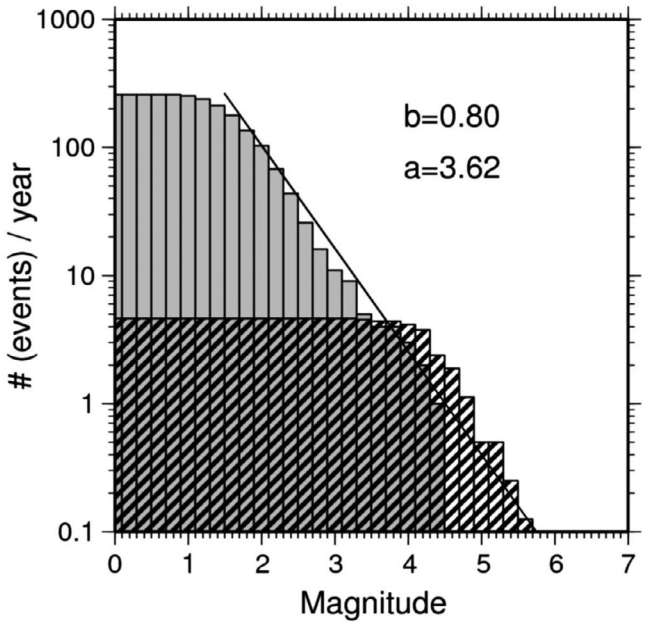

Figure 5. Comparison between the Gutenberg-Richter relation of the local magnitude measured by our temporal network and the Chilean SSN catalog data over 8 years, in the region of the network (39° to 41°S, and 74° to 71°W). The histograms show the cumulative number N of events larger than the local magnitude ML per year. The gray part of the histogram refers to the data set from the temporary network, the hatched part to the SSN data set. The regression coefficient b = 0.8 of the Gutenberg-Richter relationship $N = a - b \cdot M$ fits to both data sets. The a-value of the temporal network data is somewhat smaller than for the SSN data because no earthquakes with magnitudes ML > 4.4 were observed in the year of deployment.

Fault Zone (dashed lines in Figures 7 and 8). For the extrapolation we assumed that the VFZ continues along a straight line on the downgoing slab at the same azimuth as observed near the trench. The bending of the dashed VFZ line in Figures 7 and 8 is caused by the projection of the line from the bent plate interface to the earth surface. The Villarrica volcanic center is located above the streak between clusters A and B. It is self-evident to assume that this seismicity streak is caused by a reactivation of the incoming VFZ at depth.

[23] This idea can be tested by an analysis of focal mechanisms. A reactivated VFZ should show mainly strike-slip movement, whereas the general trend of movement along the plate interface is of thrust-type. Therefore, we determined fault plane solutions from first motion polarities and amplitude ratios between P- and S-phases observed on the vertical component. The computations were performed with the module FOCMEC of the SEISAN package [*Havskov and Ottemöller*, 1999]. The 13 most reliable resulting focal plane solutions are shown in Figure 8. Each of them is based on readings from at least 32 stations, does not show any polarity errors in its quadrants and has a well-defined orientation of the fault planes. It turned out that 85% (11/13) of these solutions have a nodal plane striking close to N70°E ("close to" meaning ±30°), which corresponds to the strike direction of the VFZ.

[24] Magma and fluid related processes are often associated with the occurrence of seismic swarms. In order to investigate the temporal behavior of cluster A we plotted the date versus the latitude for events with a hypocentral depth between 80 km and 110 km (Figure 8, bottom left). The increased seismicity between 39.3°S and 39.8°S does not show any obvious temporal variation over the observation period. There are two small time gaps in May and late June to early July which are caused by stations failure in winter time. Therefore, it seems that cluster A is a spatial but not a temporal cluster, meaning it is not a seismicity swarm.

[25] The spatial clustering between 80 km and 110 km depth is further illustrated in Figure 8 (bottom right) by histograms showing the number of events observed at three depth levels as a function of latitude. The histograms for depths shallower (50–80 km) and greater (110–140 km) than cluster A have a nearly uniform distribution of events whereas cluster A sticks out clearly as a maximum of events at 80–110 km depth between 39.3°S and 39.8°S. Hence, cluster A cannot be regarded as an artifact caused by heterogeneous network sensitivity.

4.2.2. Faulting of the Incoming Plate (Clusters C' and D)

[26] Clusters C′ and D (Figure 9a) seem to indicate faulting of the incoming plate. Cluster C′ is part of the belt of seismicity observed near the trench (C). Cluster D is located northwest of Mocha Island. The epicenters of cluster D line up parallel to the continental Mocha-Villarrica Fault mapped by *Melnick and Echtler* [2006] (Figures 1 and 9a). However, the depths of hypocenters show that the top of the cluster is subparallel to the plate interface and extends some 10 km into the subducting Nazca plate. A similar depth range of hypocenters, with respect to the top of the oceanic plate, is found for cluster C′, too. Regarding the accuracy of the location it has to be considered that the events of these clusters are far outside the network and that we cannot resolve the seismic velocity structure in 3D. Therefore, it is possible that the hypocenters show systematic errors that are difficult to assess and may exceed the errors shown in Figure 4. The systematic errors would mainly influence the depth of the events. Therefore, we cannot be sure whether cluster D occurs within the subducting slab or in the overriding plate. Still, we see the similarity in the orientation of clusters C′ and D (parallel to the isochrones of the incoming plate) as an indication that cluster D is probably in the subducting Nazca plate.

[27] Because of the limited aperture of our array it was not possible to determine reliable focal plane solutions. However, it appears plausible to relate the cluster seismicity to the bending of the oceanic plate. Both clusters show the same strike directions of ~N320°E that is parallel to the age isochrons of the incoming plate derived from magnetic mapping [e.g., *Tebbens and Cande*, 1997].

4.2.3. Offshore Seismicity in the Continental Plate (Clusters E and F)

[28] Offshore the overriding plate is nearly devoid of seismicity. An exception are clusters E and F (Figure 9b), which occur near the slip maximum of the 1960 Mw9.5 Valdivia earthquake. Cluster E is located near or just above the plate interface at 20 km depths. Cluster F occurs in the

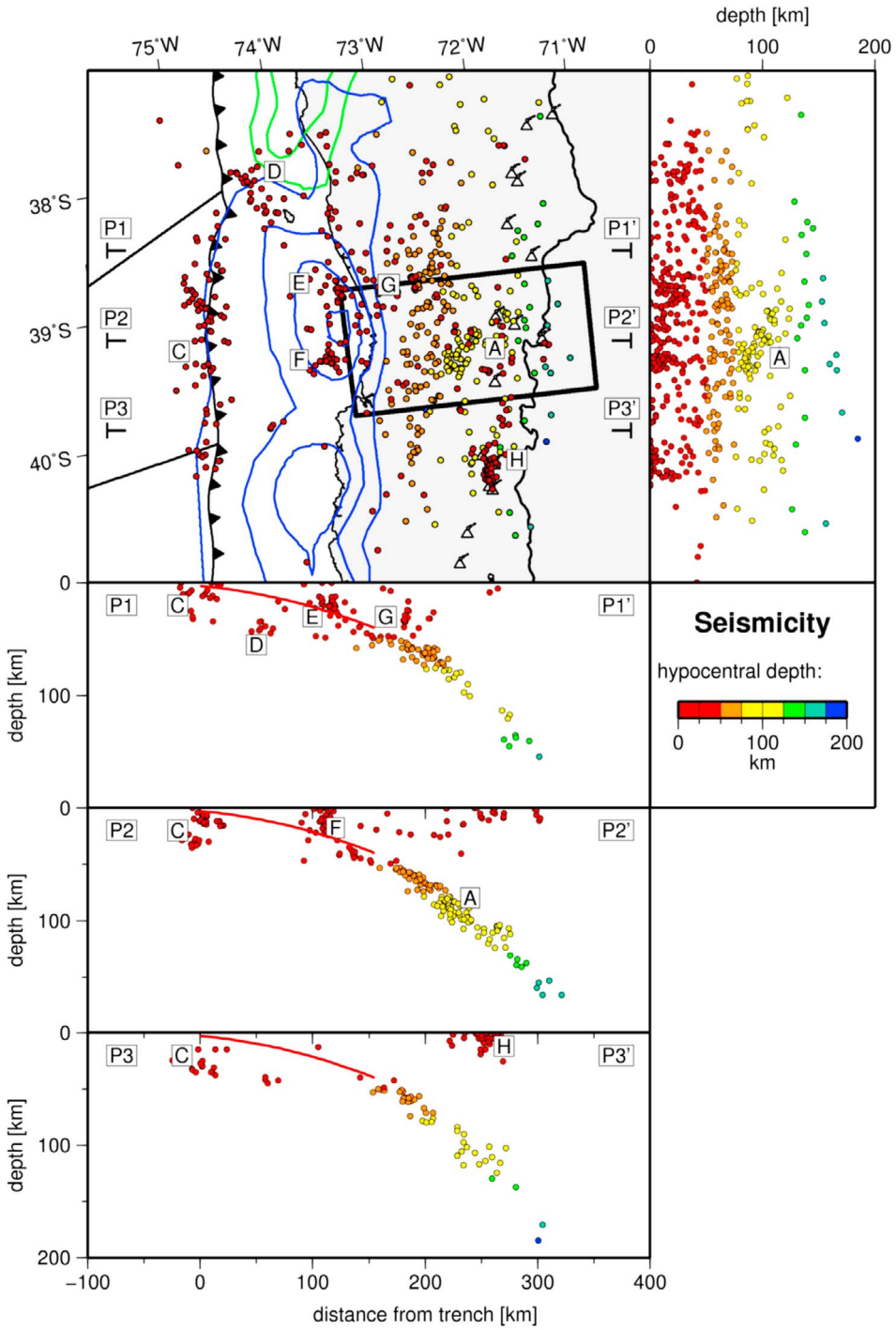

Figure 6. Single event location of seismic events (circles) observed from December 2008 to November 2009. The color code indicates hypocentral depth, the black rectangle the area covered by the seismic network. Blue and green contour lines show the slip distribution of 1960 M9.5 earthquake [*Barrientos and Ward*, 1990] and of the 2010 Maule earthquake [*Delouis et al.*, 2010]. Faults (black lines) are from *Melnick and Echtler* [2006]. The red line in the cross sections shows the plate interface. Letters A through H indicate major clusters which are also identified by double difference analysis (see text). (top left) Epicenters. (top right) Vertical plane parallel to the trench with projections of all hypocenters. (bottom figures P1 to P3) Vertical cross-sections along profiles P1 to P3 (location see top left figure) with projections of hypocenters found within 40 km wide stripes on either sides of the profiles.

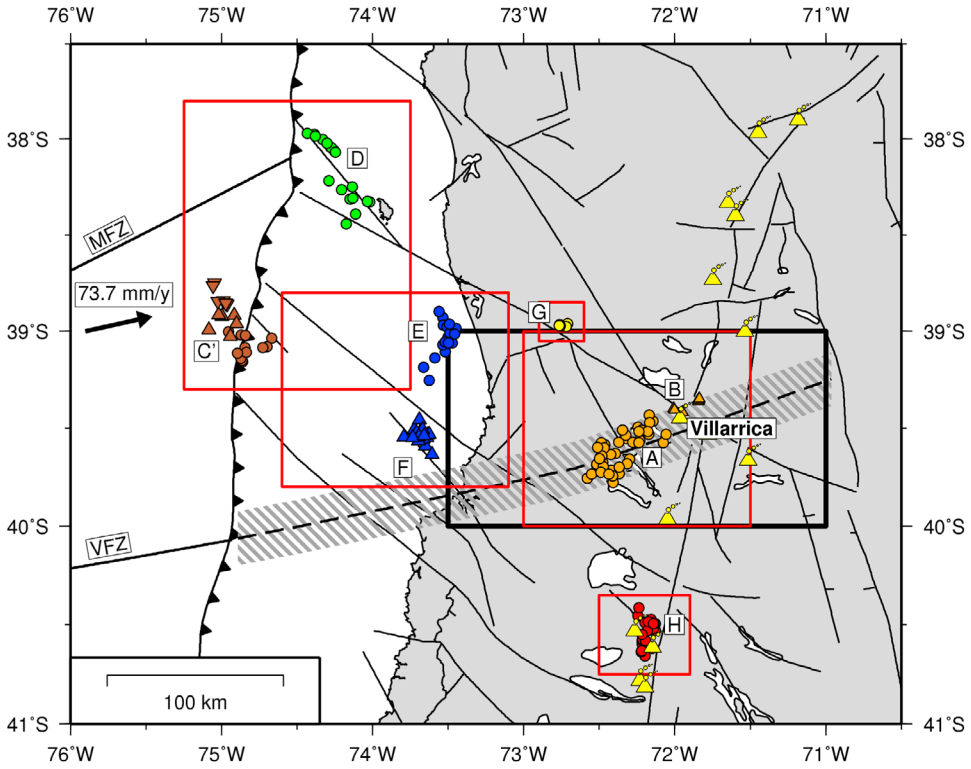

Figure 7. Overview of major spatial seismicity clusters found by cluster analysis as part of the double-difference location of events (program hypoDD by *Waldhauser* [2001]). Seismicity clusters are labeled A to G (compare Figure 6). Cluster B is considered a subcluster of A. Red boxes mark cut-outs shown in more detail in Figure 9. Black box: network area. Black solid lines: Faults after *Melnick and Echtler* [2006]; dashed line: straight line extrapolation of the Valdivia Fault Zone beneath the continent (bending of the line caused by bending of the subducted plate and projection); yellow triangles: volcanoes. VFZ - Valdivia Fault Zone, MFZ - Mocha fault Zone, V - Villarrica Volcanic Center.

crustal forearc and extends almost vertically from the surface down to the plate interface. It extends along a major NW–SE striking continental strike-slip fault that has been mapped onshore [*Melnick and Echtler*, 2006] and extrapolated offshore in Figure 9b. This fault may be regarded as the cause of the observed seismicity. Due to the limited array aperture reliable focal plane solutions could be determined for neither on the two clusters.

4.2.4. Seismicity of Continental Strike-Slip Faults (Clusters G and H)

[29] Clusters G and H (Figures 9c and 9d) are examples of the seismic activity of the major strike-slip faults leading to a segmentation of the continental plate caused by oblique plate convergence [e.g., *Melnick and Echtler*, 2006]. We are highlighting this continental fault seismicity here because it has been inferred so far from geological mapping but was not instrumentally verified in the Villarrica section of the overriding plate beforehand. Cluster G is located very close to or on the Mocha-Villarrica Fault zone at a depth of about 35 km near the Moho (Figure 9c). The absolute location error is of the order of 5 km (Figure 4). The Moho depth in that area is only poorly constrained due to the lack of deep active seismic measurements. However, tomographic studies [*Bohm*, 2004; *Haberland et al.*, 2009], a nearby receiver function profile [*Dzierma et al.*, 2012] and gravity modeling [*Alasonati Tasarova*, 2007] suggest a shallow eastward dipping Moho at 30 km to 35 km depth. Cluster H has a north–south alignment (Figure 9d). Epicenters plot at ca. 5 km distance parallel to the Liquiñe-Ofqui Fault Zone. However, since the absolute location error is of the order of 10 km (Figure 4) the earthquakes may have occurred directly on the LOFZ as well. The events are arranged almost vertically on a N–S extending fault plane (Figure 9d, right). Considering the location accuracy of ~10 km, the center of cluster H is probably located directly beneath the Puyehue-Cordón Caulle volcanic center. Puyehue volcano erupted in June 2011, ca. 2 years after cluster H was active.

5. Discussion

5.1. Significance of the Valdivia Fault Zone as a Lateral Seismic Discontinuity

[30] The major observations of our study circle around the subducted part of the Valdivia Fault Zone system, a geological unit of continental dimensions. It represents a ~2300 km long and up to ~80 km wide system of subparallel transform faults along which the oceanic lithosphere was segmentally sheared with a cumulative displacement of ~600 km [e.g., *Tebbens and Cande*, 1997]. However, according to the NUVEL-1 model of global plate tectonic motion the fault is considered to be passive today [e.g., *DeMets et al.*, 2010]. The Mocha Fault Zone can be regarded as the northern side

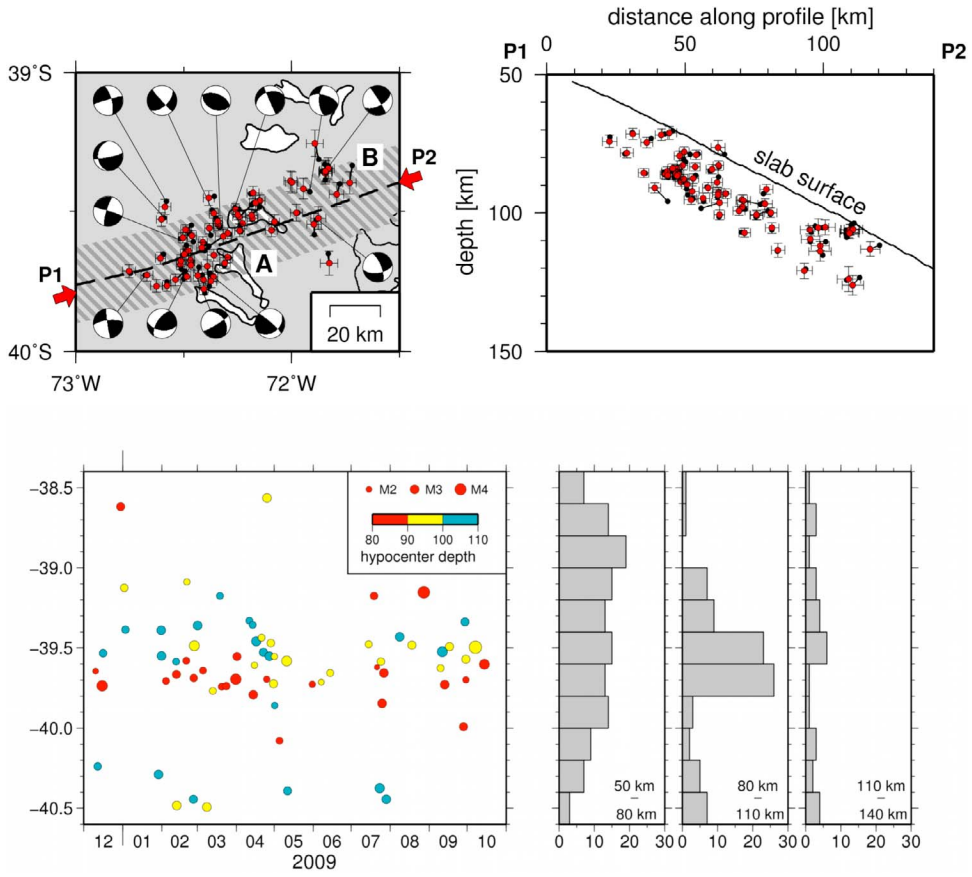

Figure 8. Detailed map view with (top left) focal plane solutions and (top right) vertical cross-section of seismic clusters A and B (cf. Figures 6 and 7) occurring along the extrapolation of the Valdivia Fault Zone (dashed line, red arrows) beneath the continent. Red circles with error bars refer to double difference relative locations, black dots to single event locations. Absolute location errors see Figure 4. Slab surface corresponds to the USGS slab 1.0 model [*Hayes et al.*, 2012]. (bottom left) Temporal and spatial distribution of the events at 80–110 km depth including cluster A between 39.4°S and 39.8°S. The size of the symbols indicates the magnitude of the events, the color the depth. (bottom right) Spatial histograms of the number of events as a function of latitude for the depth windows 50–80 km, 80–110 km (including clusters A and B) and 110–140 km.

branch of this fault system. The fault line labeled VFZ in the figures of the present article is actually the southern boundary of the fault system. Near the trench, where it enters our investigation area, it forms a singular bathymetric anomaly (see bathymetry, e.g., in *Contreras-Reyes et al.* [2010]). We are not aware of seismic studies revealing the crustal and upper mantle structure across the Valdivia Fault Zone system. However, it has been known since the 1980s that oceanic transform faults are sites where the oceanic crust is fractured, thinned and hydrated, underlain by serpentinized upper mantle [e.g., *White et al.*, 1984]. Therefore, it seems to be justified to assume that the incoming VFZ represents a site of elevated serpentinization. As such it can be expected that it differs from its surrounding rock units rheologically as well as in terms of seismic velocity. Early as well as recent seismic investigations have shown that ≥15% seismic velocity reduction, corresponding to ≥20% serpentinization, can easily be expected in fractured oceanic lithosphere [e.g., *White et al.*, 1984; *Calvert and Potts*, 1985; *Ivandic et al.*, 2010; *Dinc et al.* 2011].

5.2. State of Interplate Locking in the Region of the 1960 Slip Maximum and Influence of the Mocha and Valdivia Fracture Zones

[31] We first consider the region of the 1960 slip maximum. Although a recent reassessment of the 1960 slip distribution by *Moreno et al.* [2009] has improved the results somewhat - mainly by confining the slip to the seismogenic zone and eliminating the need for a deep zone of aseismic slip below the continent - the main features of the slip contours shown in the figures have remained largely unchanged. In particular, all inversions retain two patches of maximum coseismic slip located in the Valdivia Basin at about 39.3°S and the Puca-Trihue Basin at about 40.8°S [*Barrientos and Ward*, 1990; *Moreno et al.*, 2009], which are separated by the projected continuation of the VFZ. The location of the major southern fault trace of the VFZ is open to some uncertainty, since different positions are given in the literature. We have picked the bathymetric high and prolonged the subducted VFZ along a straight line on top of the slab, which is then projected onto the surface. This position agrees with gravity observations [*Wells et al.*, 2003].

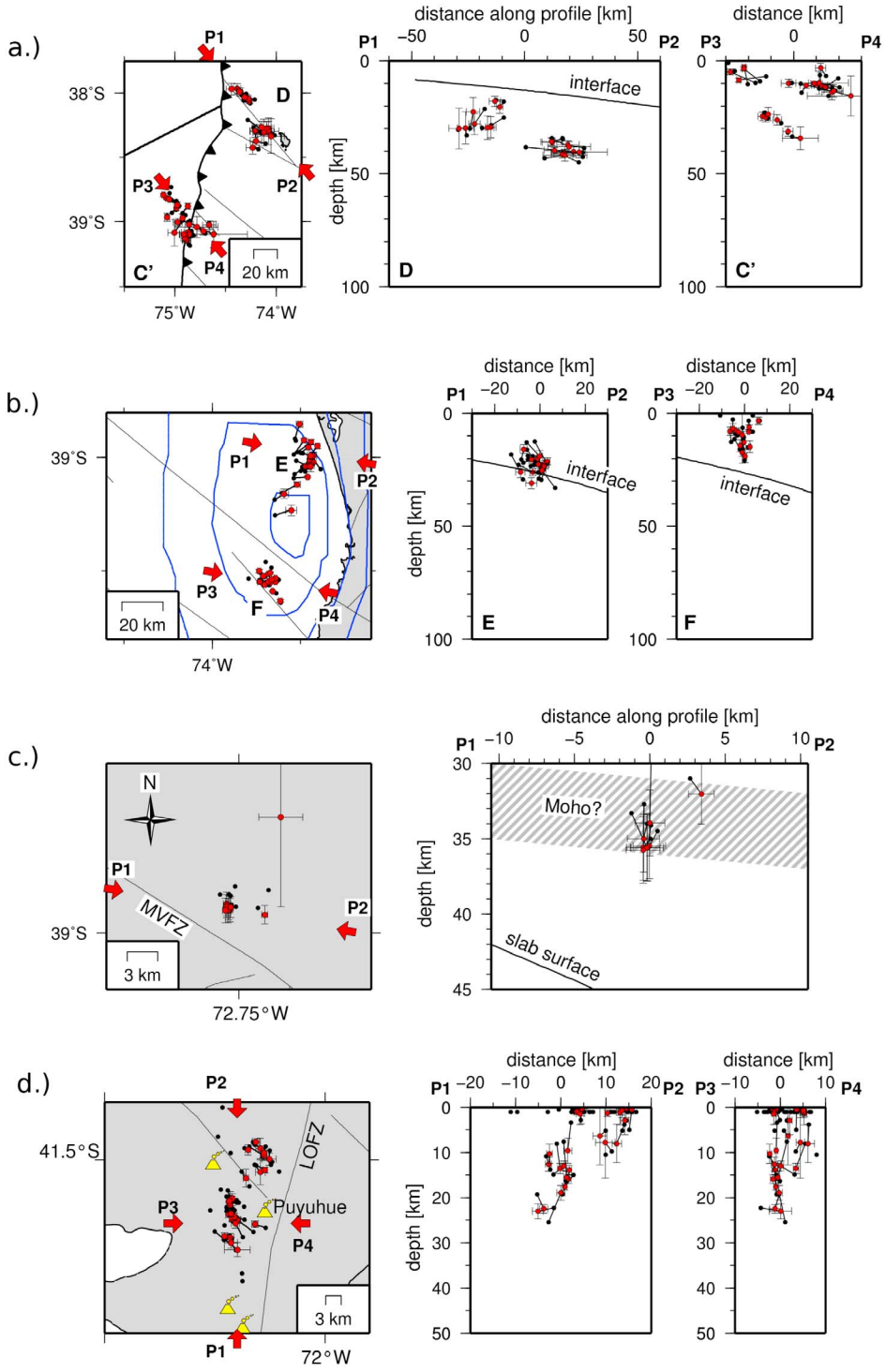

Figure 9. (left) Detailed map views and (middle and right) vertical cross-sections of seismic clusters C to H (cf. Figures 6 and 7) Red circles with error bars refer to double difference relative locations, black dots to single event locations. Absolute location errors see Figure 4. The plate interface, or slab surface, corresponds to the USGS slab 1.0 model [*Hayes et al.*, 2012]. (a) Seismic clusters C′ and occurring offshore in the downgoing plate. Clusters trend parallel to age isochrones of the incoming plate. (b) Seismic clusters E and F occurring offshore near the maximum slip area of the 1960 Mw9.5 Valdivia earthquake (blue contour lines). Cluster E appears slightly above the plate interface. Cluster F trends along a continental strike-slip fault mapped by *Melnick and Echtler* [2006]. (c) Seismic cluster G occurring near or at the continental Mocha-Villarrica strike-slip fault (MVFZ). (d) Seismic cluster H occurring near or at the left-lateral Liquiñe-Ofqui strike-slip fault (LOFZ) trending along the volcanic arc. The deeper group of events is probably centered beneath Puyehue volcano that erupted in May 2011.

[32] The fact that we observe nearly no seismicity on the plate interface of the seismogenic zone in the region of the 1960 slip may mean that either the plates are locked or aseismic slip occurs at this time. This interpretation agrees with recent GPS measurements by *Moreno et al.* [2011]. They observe complete locking (100%) in the central part of the 1960 rupture zone, but incomplete locking (25 to 60%) in the triangle formed by the VFZ and MFZ. This incomplete locking indicates increased aseismic slip. The underlying GPS velocities show a corresponding ∼50% decrease between VFZ and MFZ. From the observed seismicity, it appears that these two fracture zones significantly influence the activity and state of interplate coupling along this part of the trench.

[33] The Mocha Fracture Zone (MFZ) impinges on the trench opposite the Mocha-Villarrica Fault Zone (MVFZ), a side branch of which exhibits particularly high seismicity at depths down to 40 km (cluster D). Although the depth localization of the offshore seismicity may suffer from tradeoff effects, being outside the network, seismicity along this fault was observed at similar depths by *Haberland et al.* [2006], whose network covered the area between 37° and 39°S. The spatial coincidence of major faults in the overriding and downgoing plates, together with corresponding rheological alteration, may be the reason why both the 1960 earthquake and the 2010 Maule earthquake rupture stalled close to this feature [*Delouis et al.*, 2010; also compare *Sparkes et al.*, 2010].

[34] Between the MFZ and VFZ, nearly no seismic activity is observed on the plate interface where the 1960 slip occurred. Only the shallow seismicity of cluster E may be related to the plate interface whereas cluster F locates above the seismogenic zone. It may indicate ongoing relaxation in the overriding plate above the 1960 slip maximum, which may accommodate for the past coseismic displacement.

[35] The two patches of largest coseismic slip are divided by a local minimum along the projection of the VFZ. Assuming that incomplete plate locking were characteristic along the VFZ, the amount of accumulated strain before the 1960 earthquake would have been smaller along the VFZ trace than in the adjacent segments, leading to a locally reduced coseismic displacement.

5.3. Seismicity and Dehydration Reactions Along the Valdivia Fracture Zone

[36] The interpretation that the VFZ, passive offshore, is reactivated after subduction at a depth of 70 to 130 km is based on the coincidence that the observed seismicity cluster (Figures 7 and 8) lines up with the extrapolated VFZ and that a majority of focal plane solutions indicates strike-slip movement subparallel to this line. The mechanism behind this may be dehydration reactions in the subducting slab that weaken and reactivate the VFZ, causing enhanced seismicity. This is particularly likely since the fluid release will preferentially occur along the weakest pathways and hence favor the VFZ. Furthermore, we propose that the VFZ, as the boundary between oceanic crust created at the East Pacific Rise and the younger and hotter crust from the Chile Rise [*Tebbens et al.*, 1997], represents a strong contrast and major boundary of the incoming oceanic crust across which rheological contrasts may stimulate differential movement. This circumstance may be the reason that the VFZ appears to be much more active at greater depth than the MFZ. But this difference could also be caused by a comparatively weaker hydration of the MFZ, or simply by the observation geometry, in which the MFZ falls outside our network.

[37] Thermal modeling [*Syracuse et al.*, 2010; *van Keken et al.*, 2011] has shown that the young age and intermediate dip of the slab make the subduction zone of South Central Chile comparable to some extent to the Costa Rican subduction zone, the metamorphic reactions of which were modeled by *Peacock et al.* [2005]. They predict crust dehydration (transformation to lawsonite-amphibole eclogite) at depths of 60–100 km, which agrees with the depth range of the seismic activity along the VFZ. However, depending on the model assumption and incoming slab and sediment composition, model predictions vary considerably. *Rüpke et al.* [2002] predict deeper onset of crustal dehydration, below the observed location of the seismic cluster. Within the given uncertainties, their model is useful for a comparison of the dehydration depths from subducted sediments, crust, and serpentinized slab mantle. While the absolute depth of crustal dehydration may not be accurately known, their study shows that mantle dehydration occurs over a much smaller depth range, after crustal dehydration is nearly complete. Comparing this with the observed intermediate-depth seismicity, we suggest that the increased seismicity along the VFZ corresponds to eclogitization of the crust at 70–100 km depth, followed by mantle deserpentinization observed as a cluster of seismicity some 10–20 km deeper.

[38] The view that the subducted VFZ is a singularly strong source of released slab fluids is further supported by the presence of the Villarrica volcanic center right above the observed seismicity cluster. Villarrica volcano is one of the most active volcanoes of South America [*Stern*, 2004; *Siebert et al.*, 2010]. Isotope and trace element analysis indicate that the degree of melting and the content of slab released fluids in the melt of Villarrica volcano is at maximum for the Southern Volcanic Zone (H. Wehrmann, personal communication, 2011). In addition to providing a preferred pathway for released fluids, it appears plausible to assume that the VFZ is more strongly hydrated before subduction due to its intense fracturing and would therefore release a larger amount of fluids. The ascent of partial melt to the Villarrica volcanic center apparently follows weaknesses in the tectonic structure of the overriding plate because the volcanic center is placed at the intersection of the MVFZ and LOFZ. The depth extent of clusters G and H (Figures 9c and 9d) shows that both faults reach down to the Moho and may provide preferred magmatic pathways to the Earth's surface.

6. Conclusions

[39] We present the first observation of regional small-magnitude seismicity in the Villarrica region (39°–40°S) by a temporary local network. While statistically consistent with the Chilean National Seismological Service SSN catalog, our results permit us to observe the local seismicity of much smaller magnitudes (>2.0) and image the geometry of the Wadati-Benioff Zone from the Chile Trench down to 200 km.

[40] A gap in interplate seismicity coincides with the plate interface where the 1960 Valdivia earthquake occurred. This suggests that the plate interface in the region of maximum

1960 coseismic slip is either locked or slipping aseismically. Above the interface, two offshore seismicity clusters occur, possibly indicating ongoing stress relaxation above the maximum slip region.

[41] In the Nazca Plate, we find evidence that the subducted extension of the Valdivia Fracture Zone is reactivated beneath the volcanic arc. In particular, a seismicity cluster along the extrapolated trace of the fracture zone is observed between 70 and 100 km depth, which probably indicates weakening and reactivation of the fracture zone by dehydration reactions related to crustal eclogitization. Further dehydration, possibly due to the subducted slab mantle, may go on at greater depths, feeding the Villarrica volcanic complex that shows the highest volcanic activity in South America. The Valdivia Fracture Zone may provide a line of reduced interplate coupling, which correlates with a local minimum in the region of the 1960 slip maximum. A similar weakness may be localized at the intersection of the Mocha Fracture Zone with the trench and the Mocha-Villarrica Fracture Zone, where some seismic activity occurs in the region of overlap between the 1960 and 2010 earthquake slip contours.

[42] In contrast to the findings of *Bohm et al.* [2002] to the north of our study area (39°S), considerable crustal seismicity of small magnitude (below 3.5) is observed in the overriding plate. Most of this is localized along on- and offshore fault zones or associated with active volcanic complexes, in accordance with the observations of *Lange et al.* [2007] further south. Puyehue-Cordón Caulle might have passed through a phase of increased activity in February 2009, as observed by a swarm of seismic activity.

[43] **Acknowledgments.** This is contribution number 215 of the SFB 574 "Volatiles and Fluids in Subduction Zones" at the University of Kiel, funded by the German Research Foundation (DFG). The seismic stations were kindly provided by the GeoForschungsZentrum Potsdam instrument pool. We thank the Associate Editor and two anonymous reviewers for very insightful comments which have contributed greatly to improving this manuscript. We are indebted to the Chilean National Seismological Service for the data of 11 events included in our analysis. We thank the Chilean and Argentinian National Parks for their permission to install seismometers in the park territory. We furthermore thank all the private landowners, particularly of the Cuevas Volcánicas Villarrica, the owners of the fundos for allowing us to install the stations and keeping a good eye on the instruments, and our helper in the field work. We also thank the authors of GMT, SAC, SEISAN, PASSCAL software for the free accessibility.

References

Alasonati Tasarova, Z. (2007), Towards understanding the lithospheric structure of the southern Chilean subduction zone (36°S–42°S) and its role in the gravity field, *Geophys. J. Int.*, *170*, 995–1014, doi:10.111/j.1365-246X.2007.03466.x.

Barrientos, S. E., and S. N. Ward (1990), The 1960 Chile earthquake: Inversion for slip distribution from surface deformation, *Geophys. J. Int.*, *103*, 589–598, doi:10.1111/j.1365-246X.1990.tb05673.x.

Bohm, M. (2004), 3-D lokalbebentomographie der südlichen Anden zwischen 36° und 40°S, PhP thesis, Univ. of Kiel, Kiel, Germany.

Bohm, M., S. Lüth, H. Echtler, G. Asch, K. Bataille, C. Bruhn, A. Rietbrock, and P. Wigger (2002), The Southern Andes between 36° and 40°S latitude: Seismicity and average seismic velocities, *Tectonophysics*, *356*, 275–289, doi:10.1016/S0040-1951(02)00399-2.

Calvert, A. J., and C. G. Potts (1985), Seismic evidence for hydrothermally altered mantle beneath old crust in the Tydeman fracture zone, *Earth Planet. Sci. Lett.*, *75*, 439–449, doi:10.1016/0012-821X(85)90187-6.

Cembrano, J., and L. Lara (2009), The link between volcanism and tectonics in the southern volcanic zone of the Chilean Andes: A review, *Tectonophysics*, *471*, 96–113, doi:10.1016/j.tecto.2009.02.038.

Cembrano, J., E. Schermer, A. Laveno, and A. Sanhueza (2000), Contrasting nature of deformation along an intra-arc shear zone, the Liquiñe-Ofqui fault zone, southern Chilean Andes, *Tectonophysics*, *319*(2), 129–149, doi:10.1016/S0040-1951(99)00321-2.

Charrier, R., L. Pinto, and M. P. Rodriguez (2007), Tectonostratigraphic evolution of the Andean Orogen in Chile, in *The Geology of Chile*, edited by T. Moreno and W. Gibbons, pp. 21–114, Geol. Soc., London.

Cifuentes, I. (1989), The 1960 Chilean earthquake, *J. Geophys. Res.*, *94*(B1), 665–680, doi:10.1029/JB094iB01p00665.

Contreras-Reyes, E., E. R. Flueh, and I. Grevemeyer (2010), Tectonic control on sediment accretion and subduction off south central Chile: Implications for coseismic rupture processes of the 1960 and 2010 megathrust earthquakes, *Tectonics*, *29*, TC6018, doi:10.1029/2010TC002734.

Delouis, B., J.-M. Nocquet, and M. Vallée (2010), Slip distribution of the February 27, 2010 Mw = 8.8 Maule Earthquake, central Chile, from static and high-rate GPS, InSAR, and broadband teleseismic data, *Geophys. Res. Lett.*, *37*, L17305, doi:10.1029/2010GL043899.

DeMets, C., R. G. Gordon, and D. F. Argus (2010), Geologically current plate motions, *Geophys. J. Int.*, *181*(1), 1–80, doi:10.1111/j.1365-246X.2009.04491.x.

Dinc, A. N., W. Rabbel, E. R. Flueh, and W. Taylor (2011), Mantle wedge hydration in Nicaragua from local earthquake tomography, *Geophys. J. Int.*, *186*, 99–112, doi:10.1111/j.1365-246X.2011.05041.x.

Dzierma, Y., M. Thorwart, and W. Rabbel (2012), Moho topopgraphy and subducting oceanic slab of the Chilean continental margin in the maximum slip segment of the 1960 Mw 9.5 Valdivia (Chile) earthquake from P-receiver functions, *Tectonophysics*, *530–531*, 180–192, doi:10.1016/j.tecto.2011.12.016.

Haberland, C., A. Rietbrock, D. Lange, K. Bataille, and S. Hofmann (2006), Interaction between forearc and oceanic plate at the south-central Chilean margin as seen in local seismic data, *Geophys. Res. Lett.*, *33*, L23302, doi:10.1029/2006GL028189.

Haberland, C., A. Rietbrock, D. Lange, K. Bataille, and T. Dahm (2009), Structure of the seismogenic zone of the south central Chilean margin revealed by local earthquake traveltime tomography, *J. Geophys. Res.*, *114*, B01317, doi:10.1029/2008JB005802.

Hackney, R., et al. (2006), The segmented overriding plate and coupling at the south-central Chilean margin (36–42°S), in *The Andes: Active Subduction Orogeny*, edited by O. Oncken et al., pp. 355–374, Springer, Berlin.

Havskov, J., and L. Ottemöller (1999), SeisAn earthquake analysis software, *Seismol. Res. Lett.*, *70*, 532–534.

Hayes, G. P., D. J. Wald, and R. L. Johnson (2012), Slab1.0: A three-dimensional model of global subduction zone geometries, *J. Geophys. Res.*, *117*, B01302, doi:10.1029/2011JB008524.

Hu, Y., K. Wang, J. He, J. Klotz, and G. Khazaradze (2004), Three-dimensional viscoelastic finite element model for postseismic deformation of the great 1960 Chile earthquake, *J. Geophys. Res.*, *109*, B12403, doi:10.1029/2004JB003163.

Ivandic, M., I. Grevemeyer, J. Bialas, and C. J. Petersen (2010), Serpentinization in the trench-outer rise region offshore of Nicaragua: Constraints from seismic refraction and wide-angle data, *Geophys. J. Int.*, *180*, 1253–1264, doi:10.1111/j.1365-246X.2009.04474.x.

Khazaradze, G., K. Wang, J. Klotz, Y. Hu, and J. He (2002), Prolonged post-seismic deformation of the 1960 Chile earthquake and implications for mantle rheology, *Geophys. Res. Lett.*, *29*(22), 2050, doi:10.1029/2002GL015986.

Kissling, E., W. L. Ellsworth, D. Eberhard-Phillips, and U. Kradolfer (1994), Initial reference model in local earthquake tomography, *J. Geophys. Res.*, *99*(B10), 19,635–19,646, doi:10.1029/93JB03138.

Lange, D., A. Rietbrock, C. Haberland, K. Bataille, T. Dahm, F. Tilmann, and E. R. Flüh (2007), Seismicity and geometry of the south Chilean subduction zone (41.5°S–43.5°S): Implications for controlling parameters, *Geophys. Res. Lett.*, *34*, L06311, doi:10.1029/2006GL029190.

Lienert, B. R. E. (1991), *Report on modifications made to hypocenter, technical report, Instit. of Solid Earth Phys*, Univ. of Bergen, Bergen, Norway.

Lienert, B. R. E., and J. Havskov (1995), A computer program for locating earthquakes both locally and globally, *Seismol. Res. Lett.*, *66*, 26–36, doi:10.1785/gssrl.66.5.26.

Lienert, B. R. E., E. Berg, and L. N. Frazer (1986), Hypocenter: An earthquake location method using centered, scaled, and adaptively least squares, *Bull. Seismol. Soc. Am.*, *76*, 771–783.

Melnick, D., and H. P. Echtler (2006), Morphotectonic and geologic digital map compilations of the south-central Andes (36°–42°S), in *The Andes: Active Subduction Orogeny*, edited by O. Oncken et al., pp. 355–374, Springer, Berlin.

Moreno, M. S., J. Bolte, J. Klotz, and D. Melnick (2009), Impact of megathrust geometry on inversion of coseismic slip from geodetic data: Application to the 1960 Chile earthquake, *Geophys. Res. Lett.*, *36*, L16310, doi:10.1029/2009GL039276.

Moreno, M., et al. (2011), Heterogeneous plate locking in the south-central Chile subduction zone: Building up the next great earthquake, *Earth Planet. Sci. Lett.*, *305*(3–4), 413–424, doi:10,1016/j.epsl.2011.03.025.

Peacock, S. M., P. E. van Keken, S. D. Holloway, B. R. Hacker, G. A. Abers, and R. L. Fergason (2005), Thermal structure of the Costa Rica - Nicaragua subduction zone, *Phys. Earth. Planet. Inter.*, *149*(1–2), 187–200, doi:10.1016/j.pepi.2004.08.030.

Rehak, K., M. R. Strecker, and H. P. Echtler (2008), Morphotectonic segmentation of an active forearc, 37°–41°S, Chile, *Geomorphology*, *94*(1–2), 98–116, doi:10.1016/j.geomorph.2007.05.002.

Rosenau, M., D. Melnick, and H. Echtler (2006), Kinematic constraints on intra-arc shear and strain partitioning in the southern Andes between 38°S and 42°S latitude, *Tectonics*, *25*, TC4013, doi:10.1029/2005TC001943.

Rüpke, L. H., J. Phipps Morgan, M. Hort, and J. A. D. Connolly (2002), Are the regional variations in Central American arc lavas due to different basaltic versus peridotitic slab sources of fluids?, *Geology*, *30*(11), 1035–1038, doi:10.1130/0091-7613(2002)030<1035:ATRVIC>2.0.CO;2.

Siebert, L., T. Simkin, and P. Kimberly (2010), *Volcanoes of the World*, Univ. of Calif. Press, Berkley.

Sparkes, R., F. Tilmann, N. Hovius, and J. Hillier (2010), Subducted seafloor relief stops rupture in South American great earthquakes: Implications for rupture behaviour in the 2010 Maule, Chile earthquake, *Earth Planet. Sci. Lett.*, *298*, 89–94, doi:10.1016/j.epsl.2010.07.029.

Stern, C. R. (2004), Active Andean volcanism: Its geologic and tectonic setting, *Rev. Geol. Chile*, *31*(2), 161–206, doi:10.4067/S0716-02082004000200001.

Syracuse, E. M., P. E. van Keken, and G. A. Abers (2010), The global range of subduction zone thermal models, *Phys. Earth Planet. Inter.*, *51*(8), 1761–1782, doi:10.1016/j.pepi.2010.02.004.

Tebbens, S. F., and S. C. Cande (1997), Southeast Pacific tectonic evolution from early Oligocene to present, *J. Geophys. Res.*, *102*(B6), 12,061–12,084, doi:10.1029/96JB02582.

Tebbens, S. F., S. C. Cande, L. Kovacs, J. C. Parra, J. L. LaBrecque, and H. Vergara (1997), The Chile ridge: A tectonic framework, *J. Geophys. Res.*, *102*(B6), 12,035–12,059, doi:10.1029/96JB02581.

van Keken, P. E., B. R. Hacker, E. M. Syracuse, and G. A. Abers (2011), Subduction factory: 4. Depth-dependent flux of H_2O from subducting slabs worldwide, *J. Geophys. Res.*, *116*, B01401, doi:10.1029/2010JB007922.

Waldhauser, F. (2001), HypoDD–A program to compute double-difference hypocenter locations, *U.S. Geol. Surv. Open File Rep.*, *01–113*, 25 pp.

Waldhauser, F., and W. L. Ellsworth (2000), A double-difference earthquake location algorithm: Method and application to the northern Hayward Fault, California, *Bull. Seismol. Soc. Am.*, *90*, 1353–1368, doi:10.1785/0120000006.

Wells, R. E., R. J. Blakely, Y. Sugiyama, D. W. Scholl, and P. A. Dintermann (2003), Basin-centered asperities in great subduction zone earthquakes: A link between slip, subsidence, and subduction erosion?, *J. Geophys. Res.*, *108*(B10), 2507, doi:10.1029/2002JB002072.

White, R. S., R. S. Detrick, M. C. Sinha, and M. H. Cormier (1984), Anomalous seismic crustal structure of oceanic fracture zones, *Geophys. J. R. Astron. Soc.*, *79*, 779–798.